Journal of Membrane Science Letters 4 (2024) 100087

Contents lists available at ScienceDirect

Journal of Membrane Science Letters

journal homepage: www.elsevier.com/locate/memlet

Automated membrane characterization: In-situ monitoring of the permeate and retentate solutions using a 3D printed permeate probe device

Jonathan Aubuchon Ouimet, Faraj Al-Badani, Xinhong Liu, Laurianne Lair, Zachary W. Muetzel, Alexander W. Dowling, William A. Phillip *

Department of Chemical and Biomolecular Engineering, University of Notre Dame, Notre Dame, IN, 46556, USA

ARTICLE INFO

Keywords:
High-throughput membrane testing
3D printing
Diafiltration
Nanofiltration
Parameter estimation
Fisher information matrix

ABSTRACT

Self-driving laboratories and automated experiments can accelerate the design workflow and decrease errors associated with experiments that characterize membrane transport properties. Within this study, we use 3D printing to design a custom stirred cell that incorporates inline conductivity probes in the retentate and permeate streams. The probes provide a complete trajectory of the salt concentrations as they evolve over the course of an experiment. Here, automated diafiltration experiments are used to characterize the performance of commercial NF90 and NF270 polyamide membranes over a predetermined range of KCl concentrations from 1 to 100 mM. The measurements obtained by the inline conductivity probes are validated using offline post-experiment analyses. Compared to traditional filtration experiments, the probes decrease the amount of time required for an experimentalist to characterize membrane materials by more than 50× and increase the amount of information generated by 100×. Device design principles to address the physical constraints associated with making conductivity measurements in confined volumes are proposed. Overall, the device developed within this study provides a foundation to establish high-throughput, automated membrane characterization techniques.

Further advances across multiple scales are needed to produce solute-selective membranes for use in the wide range of applications. (Eugene et al., 2019) For instance, membranes capable of distinguishing between lithium and other monovalent ions could help intensify lithium extraction processes. (Sholl and Lively, 2016; Lair et al., 2024) Membranes capable of transporting protons, while restricting the transport of other cations, can enhance the lifetime and efficiency of redox flow batteries. (Tang and Bruening, 2020) In biomedical applications, membranes could be used to purify racemic mixtures and selectively remove low molecular weight solutes from solution (e.g., urea in dialysis). (Baker, 2023)

Principled design of fit-for-purpose membranes and processes requires relationships that bridge nanoscale and molecular design to membrane performance on the module and system scale. The solute flux, which is critical to the performance of solute-selective processes, can be described as the product of the transmembrane concentration difference and the solute permeability coefficient, B (Eq. (1)).

$$J_s = B\Delta c \tag{1}$$

In this form, information contained within B links multiple length scales. As a lumped parameter, it can inform system scale design. Alternatively, first principles can elucidate its molecular origins (Kamcev et al., 2018), provide insight into its concentration dependencies (Summe et al., 2018), and guide the reverse engineering of membrane materials. (Kitto and Kamcev, 2023) Advancing both uses requires data that captures the effect of feed concentration and composition on B. Developing these structure-property relationships will be especially important in emerging systems that tune membrane-solute interactions to achieve solute-selective separations. (Summe et al., 2018; Zofchak et al., 2022; Sheng et al., 2014; Gao et al., 2019; Wang et al., 2024)

Developing quantitative relationships between transport parameters, solution chemistry, and membrane identity can be accelerated by generating large volumes of high-fidelity data that feed into physics-based or machine learning frameworks. (Agi et al., 2024) As one example, self-driving laboratories (SDLs) combine automated experiment and characterization techniques with machine learning to determine and execute the most informative experiments. In this manner, SDLs drive material discovery and optimization while promoting an end-to-end workflow that saves time, energy, and resources.

* Corresponding author.
E-mail address: wphillip@nd.edu (W.A. Phillip).

https://doi.org/10.1016/j.memlet.2024.100087
Received 30 July 2024; Received in revised form 15 September 2024; Accepted 26 September 2024
Available online 28 September 2024

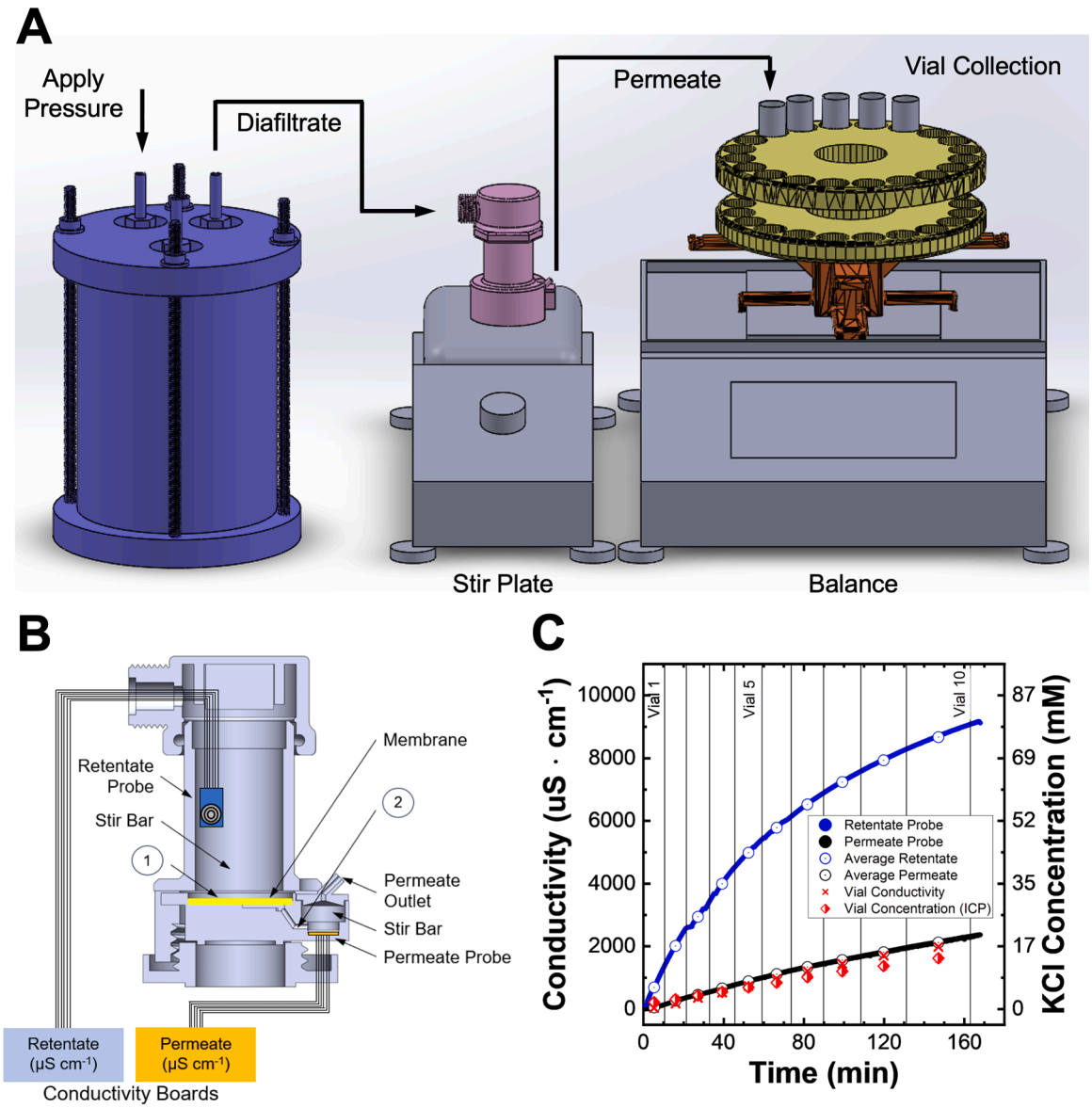

Fig. 1. *A schematic of the diafiltration apparatus.* **A.** The diafiltration apparatus is composed of three components: (1) A diafiltrate tank that contains the diafiltrate solution, (2) a modified, 3D printed stirred cell that holds a 4.1 cm^2 membrane sample, and (3) an automated vial collection system. Initially, the reservoir of the stirred cell is filled with the feed solution. Pressure is applied to the diafiltrate tank to start the experiment. The applied pressure pushes the diafiltrate solution towards the inlet of the stirred cell and drives the solution through the membrane. The diafiltration apparatus is engineered such that for every drop of solution that permeates through the membrane, one drop of diafiltrate solution enters the stirred cell. The permeate solution is collected in scintillation vials that rest on top of a balance. **B.** A cross-section of the modified stirred cell shows the placement of the conductivity probes within the retentate and permeate reservoirs. Both bulk reservoirs are well mixed by magnetic stir bars. Position #1 corresponds to the solution-membrane interface, and position #2 corresponds to the entrance of the permeate reservoir. The concentration at position #1 and position #2 are determined using the conductivity probe measurements. The solute flux is directly related to the solute concentration at these two positions. **C.** Conductivity data from the retentate and permeate probes (blue and black data points, respectively) are plotted versus time. The average concentrations of the retentate and permeate solutions for each vial are represented by the unfilled blue and black circular points, respectively. Conductivity and ICP-OES measurements for the scintillation vials, taken at the completion of the experiment, are represented as red crosses and diamonds, respectively.

(Abolhasani and Kumacheva, 2023; Seifrid et al., 2022; B. Rooney et al., 2022; MacLeod et al., 2020) A key advantage of automated experimentation is an increase in the data quality that stems from the reduction in experimental error and meticulous monitoring of experimental conditions (Mullins et al., 2024; Christopher, 2020); these benefits are critical to creating curated data sets that can be shared amongst researchers. (National Academies of Sciences, Engineering, and Medicine, 2019) To employ this paradigm to membranes, high-throughput experiments that use in-situ characterization techniques to quantify the solute flux and driving force must be developed. (Ignacz et al., 2023)

Automated diafiltration experiments can rapidly characterize membranes over predetermined ranges of concentrations. Operating in the concentrating regime, diafiltration experiments systematically dose a high-concentration diafiltrate into a stirred cell initially containing a low-concentration feed solution (Fig. 1A). (Ouimet et al., 2022; Muetzel et al., 2022; Kilmartin et al., 2021) As the experiment progresses, the flow of the diafiltrate into the retentate increases the concentration of solute within the stirred cell. By controlling the concentrations of the initial feed and diafiltrate solutions, membrane materials are characterized as the solute concentration in the retentate spans from low to high values. (Kilmartin et al., 2021) This study designs a custom stirred cell that incorporates inline conductivity probes to continuously

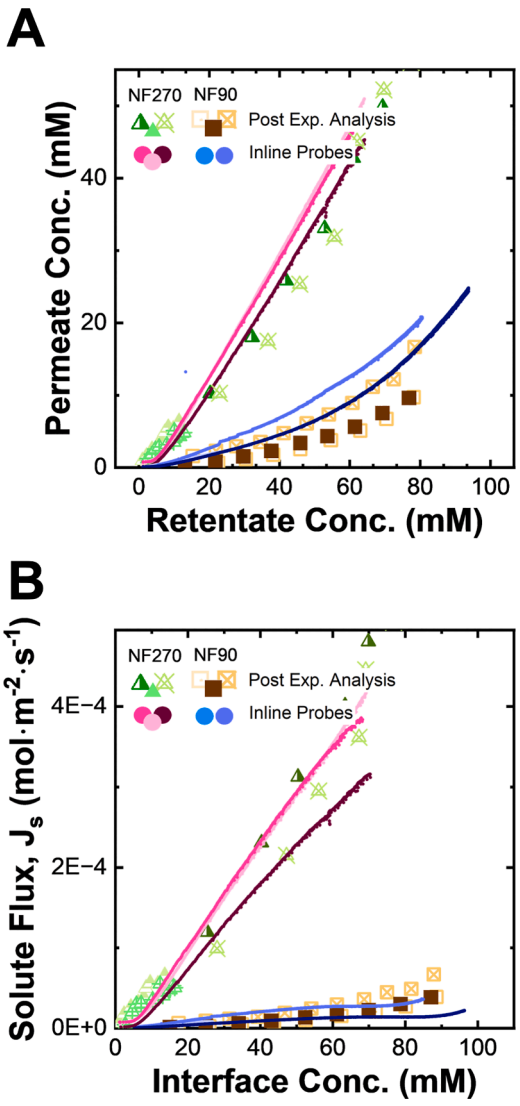

Fig. 2. *Diafiltration experiments characterizing the performance of NF90 and NF270 membranes.* The squares (NF90) (Ouimet et al., 2022) and triangles (NF270) correspond to diafiltration experiments where permeate vial concentrations were determined with ICP-OES after the experiment was completed. Every color corresponds to an experiment conducted on a unique membrane sample. The NF90 membranes were characterized using 5 mM feed & 80 mM diafiltrate KCl solutions. 1 mM/12 mM or 15 mM/120 mM KCl feed/diafiltrate solutions were used to characterize the NF270 membranes. Data obtained from the permeate probe apparatus are represented by circular data points (NF90: shades of blue, NF270: shades of pink). Within the experiments that used a permeate probe, a 1 mM KCl feed and 80 mM KCl diafiltrate was used to characterize both the NF90 and NF270 membranes. Experimentally measured concentration data are plotted within Panel **A**. To account for the effect of water flux, Panel **B** compares the solute flux ($J_s \cong J_w c_p$) as a function of the interface concentration.

monitor the concentration of these solutions to reduce the time demand on experimentalists and increase the amount of information generated.

3D printing enables the creation of a custom stirred cell with integrated sensors. Fig. 1B presents a cross section of the stirred cell that was created to possess inline retentate and permeate conductivity probes. Four electrode LFS conductivity probes, which were selected for their compact design, enable conductivity measurements within small solution volumes. The custom stirred cell, and all associated parts, were designed in SolidWorks and printed on a FormLabs 3+ resin printer. A link to the GitHub repository with editable SolidWorks files, information on print orientation (Fig. S1), post-processing steps (Fig. S2), and device assembly (Fig. S3) is provided in the Supplementary Information.

The data generated by the inline conductivity probes is corroborated by measurements obtained from analyzing aliquots of the permeate and retentate solution after an experiment concludes. A diafiltration experiment that used a 1 mM KCl feed and 100 mM KCl diafiltrate to characterize an NF90 membrane demonstrates this validation (Fig. 1C). Details regarding the experimental procedure are included within the Supplementary Information. During this experiment, the conductivity probe readings were recorded at 5-second intervals. Additionally, 10 scintillation vials, each possessing 1.00±0.05 g of solution, were collected. As the experiment progresses, the time necessary to fill each vial increases (Fig. 1C, vertical lines). This increase is attributed to an increase in the osmotic pressure of the retentate, and consequently a decrease in the volumetric water flux. After the experiment, the KCl concentration in each vial was determined using conductivity (red crosses) and inductively coupled plasma optical emission spectroscopy (ICP OES) (red diamonds). The concentrations obtained by analyzing the scintillation vials closely align with the data from the inline conductivity probe (black data points).

Fig. 2A extends this analysis to multiple membrane samples. Here, the retentate and permeate concentrations are reported on the horizontal and vertical axes, respectively. The square data points correspond to triplicate experiments previously reported in literature. (Ouimet et al., 2022) For each data set, the permeate concentration is obtained by analyzing the scintillation vials after the experiment, and the retentate concentration is calculated from the volume average concentration of the retentate conductivity. Experiments conducted with the inline conductivity probes are graphed as circular data points with the shades of blue representing experiments on two distinct membranes. The high density of data makes the points appear as a solid line. The vertical scatter between the membrane samples is likely due to differences in the volumetric flux, J_w. One way to account for the influence of J_w on the data is to compare J_s as a function of the interface concentration on the upstream side of the membrane. Here, the interface concentration is calculated using a thin film model that accounts for the effects of concentration polarization (see Supporting Information). By comparing the solute flux as a function of the interface concentration, the data sets collapse on top of one another (Fig. 2B). To ensure this trend was consistent across membranes with varying hydraulic permeabilities, the same analysis was conducted on commercial NF270 membranes, which possess hydraulic permeabilities that are 4× higher than the NF90 membrane (i.e., NF90: 3 L m^{-2} h^{-1} bar^{-1} and NF270: 12 L m^{-2} h^{-1} bar^{-1}). The crossed, dotted, and partially-filled triangles correspond to three NF270 membranes where the permeate vials were analyzed after the experiment; the circular data points (various shades of pink) correspond to data obtained with the inline probes. The close alignment between the *in-situ* and post-experiment analyses across membrane types and samples validates the permeate probe device.

A unique strength of the permeate probe device is the generation of data at low retentate concentrations. Understanding the phenomena that govern membrane-solute interactions in dilute solutions is important when target solutes are found at trace concentrations, e.g., lithium recovery (Lair et al., 2024). When the permeate probe is not used, the concentration measured for each vial represents an average over all the permeate fluid collected. Therefore, the retentate conductivity data must be reduced to a volume average measurement to correlate it with the permeate concentration (Fig. 2, square and triangular data). This data reduction hinders membrane characterization at low concentrations. For instance, when characterizing NF90 membranes using a 5 mM KCl feed and 80 mM KCl diafiltrate, the average retentate concentration of the first vial was ~15 mM (Fig. 2). Similar trends are seen in the data for the NF270 membrane. While additional experiments with a 1 mM KCl feed and a 12 mM KCl diafiltrate (Fig. 2, lime green triangles) could be performed, the implementation of the permeate probe provides an equal number of measurements for both solutions enabling the full trajectory of membrane performance to be obtained in a single

Table 1
The FIM, and its corresponding eigenvalues and eigenvectors, are calculated for a diafiltration experiment. Two different data sets are used to analyse the experiment. The first data set includes the inline permeate conductivity probe data, the second data set omits the permeate probe data and only uses the ICP OES measurements to obtain the permeate vial concentrations.

Data Set	FIM ($\times 10^6$)			Eigenvalues ($\times 10^6$)	Eigenvectors		
	L_p	B	σ		L_p	B	σ
Inline Permeate Probe	7.55	89.86	−9.75	2.71	[0.98	−0.03	0.17]
	89.86	2960.60	79.27	74.86	[0.17	0.02	−0.98]
	−9.75	79.27	74.91	2965.49	[0.03	1	0.03]
ICP-OES	4.43	4.42	−13.51	0.89	[0.88	0.34	0.34]
	4.42	23.48	−33.96	6.73	[0.45	−0.82	−0.35]
	−13.51	−33.96	69.61	89.89	[0.16	0.46	−0.87]

experiment.

In addition to the high density of data generated, the permeate probe device dramatically reduces the time it takes an experimenter to characterize a membrane (Table S1). For instance, it takes an experimenter approximately 47 h to characterize ion permeation through an NF90 membrane using traditional filtration experiments. (Ouimet et al., 2022) By conducting a diafiltration experiment with the permeate probe device, characterizing the transport parameters of the same membrane can require as little as 40 min (Table S1). Automating data collection and analysis results in a more than 50× decrease in the time required by an experimentalist. The automated vial collection system means that an experimentalist does not need to be present throughout the course of an experiment and, for single salt studies, the continuous monitoring of the retentate and permeate conductivities removes the need to prepare samples for post-experiment analysis. Due to the automated data collection, the experiments generate curated data sets. Specifically, an in-house MATLAB code was created to process the data and account for the lag between the permeate conductivity reading and the permeate collected within each vial. Processing data in this manner further decreases the time requirements on the experimentalist.

Generating high-density data sets in a rapid manner also reduces the uncertainty associated with regressing transport parameters. To illustrate this, the transport parameters for an NF90 membrane characterized with a 1 mM KCl feed and 100 mM KCl diafiltrate (Fig. 1C) were regressed (Table S2) using two data set variations (Ouimet et al., 2022; Liu et al., 2022); the first data set uses the inline conductivity measurements provided by the permeate probe, the second set omits the conductivity measurements and uses ICP-OES analysis. Importantly, the hydraulic permeability, L_p, solute permeability coefficient, B, and reflection coefficient, σ, regressed within this study ($L_p = 3.56$ L m^{-2} h^{-1} bar^{-1}, $B = 0.22$ μm s^{-1}, and $\sigma = 1$) closely align with regressed parameters from previous studies ($L_p = 3.18$ - 4.37 L m^{-2} h^{-1} bar^{-1}, $B = 0.31$ - 0.78 μm s^{-1} and $\sigma = 1$). (Ouimet et al., 2022; Al-Zoubi et al., 2007) The Fisher information matrices (FIMs) (Rothenberg, 1971; Franceschini and Macchietto, 2008; Befort et al., 2023; Wang and Dowling, 2022) and their eigen decompositions for the two variations are compared in Table 1. All of the elements of the FIMs are larger for the data set that uses the inline permeate probe indicating that the probe measurements provide information that is not contained within the ICP-OES data set.

Analysing the eigen decomposition of the FIM indicates which parameter can be reliably estimated. For example, the largest eigenvalue for the permeate probe data set is 2.97×10^9 and its corresponding eigenvector is in the direction of parameter B. This indicates B can be estimated with the greatest precision. Similarly, in the data set that only uses ICP-OES measurements, the eigenvalue of 6.73×10^6 is predominantly in the direction of B.

Comparing the ratio of these eigenvalues reveals data obtained from the permeate probe contains (2965.49/6.73 ≈) 440 times more information about B than using only ICP-OES measurements. Similarly, the permeate probe data contains (2.71/0.89 ≈) 3.0 and (74.86/89.89 ≈) 0.83 times the information about L_p and σ, respectively.[1] The significant improvement in information content indicates that incorporating the permeate probe reduces the uncertainty associated with regressing the transport parameters. Improved precision, especially for the solute permeability coefficient, will be critical as researchers engineer nanoscale membrane-solute interactions to create solute selective membranes.

Model-based design of experiments (MBDoE) frameworks select the optimal sequence of experiments to increase parameter precision. (Wang and Dowling, 2022) MBDoE practitioners choose between a handful of optimality criteria, i.e., functions that convert the FIM into a scalar measure of information content. These criteria, and gains in information associated with each, are discussed within the supplementary information (Table S3).

The permeate probe device was carefully engineered to ensure that the advantages detailed above could be leveraged to their fullest. Achieving this aim required designing around the physical constraints associated with making accurate conductivity measurements in small volumes. Specifically, a minimum volume of solution (~100 μL) above the sensor is required by the manufacturer. (Schonstein et al) Our experiments also demonstrate that this reservoir should be well-mixed. Both criteria are met within the design presented in Fig. S4. Solution that permeates through the membrane is directed to a reservoir that contains the conductivity probe and a stir bar. The stir bar is essential to keeping the solution well mixed (Fig. S5). Importantly, the stir bar is positioned so that its magnetic field does not influence the conductivity readings. For this device, the magnetic field decays as r^{-3} where r is the radius of the stir bar magnet. (Thomaszewski et al., 2008; Ziff-Davis Publishing 1983) Consequently, the stir bar is placed 2.8 mm (~3.5 radii) away from the conductivity probe (Fig. S6). Additionally, to minimize bubble formation, the stir bar is held in a custom, plasma-treated holder (Fig. S7).

With the device geometry established and performance validated, we turn our attention to relating the flux of solute to the diffusive driving force across the membrane, Eq. (1). The concentration of ions at the membrane-solution interface (position 1) and downstream permeate (position 2) must be known to calculate the diffusive driving force. The interface concentration accounts for the effects of concentration polarization and can be calculated from the retentate concentration using a thin film model. (Zeman and Zydney, 2017) The concentration of the permeate solution entering the reservoir can be calculated using a mass balance that relates it to the conductivity of the solution measured by the probe.

The start-up process for a filtration experiment illustrates the

[1] We caution these information gains are approximations. For example, accounting for any time-series correlations in the measurement error of the conductivity probes will likely decrease information gains.

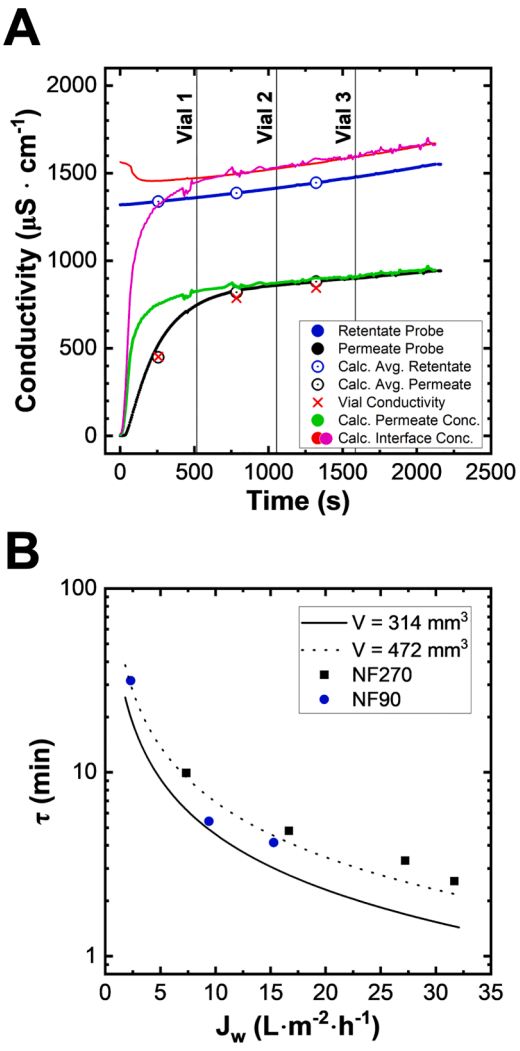

Fig. 3. *Filtration experiments validate the device residence time.* **A.** A representative NF270 filtration experiment with a 10 mM KCl feed at 2 bar. The two inline probes measure the bulk retentate (blue circles) and permeate (black circles) conductivity values. The end of each vial is indicated by the vertical lines. For each vial, the volume-averaged conductivity measurements are represented by the open circles. The conductivity of the scintillation vials (red crosses) are obtained after the experiment. The concentration of solution entering the permeate reservoir (green data points) is calculated using the residence time correlation (Eq. (3)). The concentration at the retentate-membrane interface is calculated using two methods. (i) The red data points use a thin film model. (ii) The magenta data points use the sieving coefficient and concentration of solution entering the permeate reservoir. **B.** Experimental residence times (data points) are compared to values calculated using the membrane area, water flux, and reservoir volume (lines). Filtration experiments were conducted on NF90 and NF270 membranes operating at applied pressures between 1 and 4 bar. A volume of 314 mm^3 corresponds to the permeate reservoir. A volume of 472 mm^3 includes the permeate reservoir and the collection wells under the membrane (see Fig. S4).

importance of this consideration (Fig. 3). Before the experiment starts, the permeate reservoir is rinsed with DI water resulting in an initial conductivity reading less than 20 μS cm^{-1}. Subsequently, a 10 mM KCl feed solution is placed in the reservoir of the stirred cell and pressurized. As the solution permeates through the membrane, the DI water in the permeate reservoir is displaced by KCl-containing permeate. As a result, the conductivity measurement increases sharply during the initial 500 s (Fig. 3A, black line). This transition is not instantaneous; a finite amount of time is required for the KCl-containing permeate to reach the sensing chamber and displace the DI water. The gradual increase in the permeate concentration after this initial period is driven by the increasing retentate concentration. Over the course of the filtration experiment, the retentate concentration increases by ~15% because the membrane retains KCl (rejection ~40%) and the volume of the retentate solution decreases.

A mass balance is written (Eq. (2)) to calculate the initial lag associated with displacing the DI water in the reservoir.

$$\frac{d(V_p c_p)}{dt} = J_w A_m c_p^{L_s} - J_w A_m c_p \tag{2}$$

$$c_p^{L_s} = \frac{V_p}{J_w A_m}\frac{dc_p}{dt} + c_p \tag{3}$$

Here, $c_p^{L_s}$ and c_p are the concentration of the solution entering the reservoir and the concentration measured by the conductivity probe, respectively. V_p is the volume of the permeate reservoir and A_m is the membrane area. Because V_p is constant, Eq. (2) can be rearranged (Eq. (3)) to demonstrate that the residence time, $\tau = \frac{V_p}{J_w A_m}$, defines the response rate of the reservoir. Reassuringly, in the limit that $V_p \to 0$, and thus $\tau \to 0$, there is no lag, and $c_p^{L_s} = c_p$.

The residence time of the permeate probe device was validated using a series of filtration experiments. The regressed value of τ (see SI for discussion) is compared to the residence time determined from the cell geometry in Fig. 3B. Experiments were conducted on NF90 and NF270 membranes at a range of applied pressures to span volumetric fluxes between 2 – 32 L m^{-2} h^{-1}. The regressed τ values closely match theoretical residence times Fig. 3B, confirming that Eq. (3) can be used to calculate the concentration of ions entering the permeate reservoir. Furthermore, these results demonstrate that for thin membranes, the residence time in the reservoir is much greater than the characteristic time associated with solute transport through the membrane ($\tau_{membrane}$). Specifically, while the residence time of the reservoir was on the order of 1–100 min, for nanofiltration membranes that are several hundred nanometers thick with B ~0.2 μm·s^{-1}, (Ouimet et al., 2022) $\tau_{membrane} < 1$ s. Therefore, the membrane can be assumed to operate at pseudo-steady state.

The field of membrane separations is poised to experience a paradigm shift in which automated experimentation and data science will increase the rate of material and process discovery. Here, 3D printing allowed for the creation of a custom stirred cell device that overcomes the physical constraints associated with making accurate conductivity measurements in small volumes. When combined with automated diafiltration experiments, the device can systematically explore membrane performance over a wide concentration range. As such, the work outlined here provides a foundation for automating membrane characterization techniques and creating self-driving laboratories.

Funding sources

This work was kindly support by the National Science Foundation (NSF) through award 2147605. JAO acknowledges support from the CEST/Bayer Predoctoral Fellowship and the Patrick and Jana Eilers Graduate Research Student Fellowship for Energy Related Research at the University of Notre Dame. The authors acknowledge the Center for Engineering and Technology (CEST) for the use of instruments to perform experimental analyses.

CRediT authorship contribution statement

Jonathan Aubuchon Ouimet: Writing – review & editing, Writing – original draft, Methodology, Formal analysis, Data curation, Conceptualization. **Faraj Al-Badani:** Writing – review & editing, Methodology. **Xinhong Liu:** Writing – review & editing, Formal analysis, Data curation. **Laurianne Lair:** Writing – review & editing. **Zachary W. Muetzel:** Conceptualization. **Alexander W. Dowling:** Writing – review & editing,

Conceptualization. **William A. Phillip:** Writing – review & editing, Funding acquisition, Conceptualization.

Declaration of competing interest

The authors declare that they have no known competing financial interests or personal relationships that could have appears to influence the work reported in this paper.

Data availability

Data will be made available on request.

Acknowledgments

This work was kindly support by the National Science Foundation (NSF) through award 2147605. JAO acknowledges support from the CEST/Bayer Predoctoral Fellowship and the Patrick and Jana Eilers Graduate Research Student Fellowship for Energy Related Research at the University of Notre Dame. L.L. received support from a Graduate Assistance in Areas of National Need fellowship from the Department of Education via Grant P200A210048 and the Remick Graduate Fellowship in Engineering administered by the University of Notre Dame. The authors acknowledge the Center for Engineering and Technology (CEST) for the use of instruments to perform experimental analyses. The authors gratefully acknowledge Jonathan Hickle for the SolidWorks modeling within Fig. 1A.

Supplementary materials

Supplementary material associated with this article can be found, in the online version, at doi:10.1016/j.memlet.2024.100087.

References

Abolhasani, M., Kumacheva, E., 2023. The rise of self-driving labs in chemical and materials sciences. Nat. Synth. 2 (6), 483–492. https://doi.org/10.1038/s44160-022-00231-0.

Agi, D.T., Jones, K.D., Watson, M.J., Lynch, H.G., Dougher, M., Chen, X., Carlozo, M.N., Dowling, A.W., 2024. Computational toolkits for model-based design and optimization. Curr. Opin. Chem. Eng. 43, 100994. https://doi.org/10.1016/j.coche.2023.100994.

Al-Zoubi, H., Hilal, N., Darwish, N.A., Mohammad, A.W., 2007. Rejection and modelling of sulphate and potassium salts by nanofiltration membranes: neural network and Spiegler-Kedem model. Desalination 206 (1–3), 42–60. https://doi.org/10.1016/j.desal.2006.02.060.

Baker, R.W., 2023. Membrane Technology and Applications. John Wiley & Sons.

Befort, B.J., Garciadiego, A., Wang, J., Wang, K., Franco, G., Maginn, E.J., Dowling, A. W., 2023. Data science for thermodynamic modeling: case study for ionic liquid and hydrofluorocarbon refrigerant mixtures. Fluid Phase Equilib. 572, 113833. https://doi.org/10.1016/j.fluid.2023.113833.

Christopher, P., 2020. Automating academic laboratories: promoting reliability, productivity, and safety. ACS Energy Lett. 5 (8), 2737–2738. https://doi.org/10.1021/acsenergylett.0c01644.

Eugene, E.A., Phillip, W.A., Dowling, A.W., 2019. Data science-enabled molecular-to-systems engineering for sustainable water treatment. Curr. Opin. Chem. Eng. 26, 122–130. https://doi.org/10.1016/j.coche.2019.10.002.

Franceschini, G., Macchietto, S., 2008. Model-based design of experiments for parameter precision: state of the art. Chem. Eng. Sci. 63, 4846–4872. https://doi.org/10.1016/j.ces.2007.11.034.

Gao, F., Hunter, A., Qu, S., Hoffman, J.R., Gao, P., Phillip, W.A., 2019. Interfacial junctions control electrolyte transport through charge-patterned membranes. ACS Nano 13 (7), 7655–7664. https://doi.org/10.1021/acsnano.9b00780.

Ignacz, G., Beke, A.K., Szekely, G., 2023. Data-driven future for nanofiltration: escaping linearity. J. Membr. Sci. Lett. 3 (1), 100040. https://doi.org/10.1016/j.memlet.2023.100040.

Kamcev, J., Paul, D.R., Manning, G.S., Freeman, B.D., 2018. Ion diffusion coefficients in ion exchange membranes: significance of counterion condensation. Macromolecules 51 (15), 5519–5529. https://doi.org/10.1021/acs.macromol.8b00645.

Kilmartin, C.P., Ouimet, J.A., Dowling, A.W., Phillip, W.A., 2021. Staged diafiltration cascades provide opportunities to execute highly selective separations. Ind. Eng. Chem. Res. 60 (43), 15706–15719. https://doi.org/10.1021/acs.iecr.1c02984.

Kitto, D., Kamcev, J., 2023. The need for ion-exchange membranes with high charge densities. J. Memb. Sci. 677, 121608. https://doi.org/10.1016/j.memsci.2023.121608.

Lair, L., Ouimet, J.A., Dougher, M., Boudouris, B.W., Dowling, A.W., Phillip, W.A., 2024. Critical mineral separations: opportunities for membrane materials and processes to advance sustainable economies and secure supplies. Annu. Rev. Chem. Biomol. Eng. https://doi.org/10.1146/annurev-chembioeng-100722-114853.

Liu, X., Wang, J., Ouimet, J.A., Phillip, W.A., Dowling, A.W, 2022. Membrane characterization with model-based design of experiments. In: Yamashita, Y., Kano, M. (Eds.), Computer Aided Chemical Engineering, Computer Aided Chemical Engineering, 49. 14 International Symposium on Process Systems Engineering; Elsevier, pp. 859–864. https://doi.org/10.1016/B978-0-323-85159-6.50143-3.

MacLeod, B.P., Parlane, F.G.L., Morrissey, T.D., Häse, F., Roch, L.M., Dettelbach, K.E., Moreira, R., Yunker, L.P.E., Rooney, M.B., Deeth, J.R., Lai, V., Ng, G.J., Situ, H., Zhang, R.H., Elliott, M.S., Haley, T.H., Dvorak, D.J., Aspuru-Guzik, A., Hein, J.E., Berlinguette, C.P., 2020. Self-driving laboratory for accelerated discovery of thin-film materials. Sci. Adv. 6 (20), eaaz8867. https://doi.org/10.1126/sciadv.aaz8867.

Muetzel, Z.W., Ouimet, J.A., Phillip, W.A., 2022. Device for the acquisition of dynamic data enables the rapid characterization of polymer membranes. ACS Appl. Polym. Mater 4 (5), 3438–3447. https://doi.org/10.1021/acsapm.2c00048.

Mullins, N., Babamova, I., de Lannoy, C.-F., Latulippe, D.R., 2024. Low-cost automated flat-sheet membrane casting: an open-source, advanced manufacturing approach. J. Membr. Sci. Lett. 4 (1), 100075. https://doi.org/10.1016/j.memlet.2024.100075.

National Academies of Sciences, Engineering, and Medicine, A Research Agenda for Transforming Separation Science, 2019. National Academies Press.

Ouimet, J.A., Liu, X., Brown, D.J., Eugene, E.A., Popps, T., Muetzel, Z.W., Dowling, A.W., Phillip, W.A, 2022. DATA: diafiltration apparatus for high-throughput analysis. J. Memb. Sci. 641, 119743. https://doi.org/10.1016/j.memsci.2021.119743.

Rooney, M.B., MacLeod, B.P., Oldford, R., Thompson, Z.J., White, K.L., Tungjunyatham, J., Stankiewicz, B.J., Berlinguette, C.P., 2022. A self-driving laboratory designed to accelerate the discovery of adhesive materials. Digit. Discov. 1 (4), 382–389. https://doi.org/10.1039/D2DD00029F.

Rothenberg, T.J., 1971. Identification in parametric models. Econometrica 39 (3), 577–591. https://doi.org/10.2307/1913267.

Schonstein, T. LFS 1107 - Minimum Solution Requirements.

Seifrid, M., Pollice, R., Aguilar-Granda, A., Morgan Chan, Z., Hotta, K., Ser, C.T., Vestfrid, J., Wu, T.C., Aspuru-Guzik, A., 2022. Autonomous chemical experiments: challenges and perspectives on establishing a self-driving lab. Acc. Chem. Res. 55 (17), 2454–2466. https://doi.org/10.1021/acs.accounts.2c00220.

Sheng, C., Wijeratne, S., Cheng, C., Baker, G.L., Bruening, M.L., 2014. Facilitated ion transport through polyelectrolyte multilayer films containing metal-binding ligands. J. Memb. Sci. 459, 169–176. https://doi.org/10.1016/j.memsci.2014.01.051.

Sholl, D.S., Lively, R.P., 2016. Seven chemical separations to change the world. Nature 532 (7600), 435–437. https://doi.org/10.1038/532435a.

Summe, M.J., Jagriti Sahoo, S., Whitmer, J.K., Phillip, W.A., 2018. Salt permeation mechanisms in charge-patterned mosaic membranes. Molecul. Syst. Des. Eng. 3 (6), 959–969. https://doi.org/10.1039/C8ME00061A.

Tang, C., Bruening, M.L., 2020. Ion separations with membranes. J. Polym. Sci. 58 (20), 2831–2856. https://doi.org/10.1002/pol.20200500.

Thomaszewski, B., Gumann, A., Pabst, S., Straßer, W., 2008. Magnets in motion. ACM Trans. Graph 27 (5), 162. https://doi.org/10.1145/1409060.1409115, 1-162:9.

Wang, J., Dowling, A.W, 2022. Pyomo.DOE: an open-source package for model-based design of experiments in python. AIChE J. 68 (12), e17813. https://doi.org/10.1002/aic.17813.

Wang, J., Dong, D., Lair, L., Yaroshchuk, A., Phillip, W.A., Bruening, M.L., 2024. Combined nanofiltration and diafiltration for isolation of rare-earth ions. J. Memb. Sci. 711, 123173. https://doi.org/10.1016/j.memsci.2024.123173.

Zeman, L.J., Zydney, A., 2017. Microfiltration and Ultrafiltration: Principles and Applications, 618. https://doi.org/10.1201/9780203747223.

Ziff-Davis Publishing, 1983. Electronic Experimenter's Handbook 1984, 1983.

Zofchak, E.S., Zhang, Z., Marioni, N., Duncan, T.J., Sachar, H.S., Chamseddine, A., Freeman, B.D., Ganesan, V, 2022. Cation–ligand interactions dictate salt partitioning and diffusivity in ligand-functionalized polymer membranes. Macromolecules 55 (6), 2260–2270. https://doi.org/10.1021/acs.macromol.2c00035.